China Ocean Eng., Vol. 29, No.1, pp. 17 – 32

DOI 10.1007/s13344-015-0002-6, ISSN 0890-5487

Motion Characteristics of Cavitation Bubble near the Rigid Wall with the Driving of Acoustic Wave*

YE Xi (叶　曦)[a], ZHANG A-man (张阿漫)[a, 1] and ZENG Dong-rui (曾冬瑞)[b]

[a] *College of Shipbuilding Engineering*, *Harbin Engineering University*, *Harbin 150001*, *China*

[b] *College of Mathematics*, *Nanjing University*, *Nanjing 210046*, *China*

(Received 26 May 2013; received revised form 25 October 2013; accepted 20 January 2014)

ABSTRACT

The dynamics of cavitation bubble is analyzed in the compressible fluid by use of the boundary integral equation considering the compressibility. After the vertical incidence of plane wave to the rigid wall, the motion characteristics of single cavitation bubble near the rigid wall with initial equilibrium state are researched with different parameters. The results show that after the driving of acoustic wave, the cavitation bubble near the rigid wall will expand or contract, and generate the jet pointing to the wall. Also, the existence of the wall will elongate time for one oscillation. With the compressible model, the oscillation amplitude is reduced, as well as the peak value of inner pressure and jet tip velocity. The effect of the wall on oscillation amplitude is limited. However with the increment of initial vertical distance, the effect of wall on the jet velocity is from acceleration to limitation, and finally to acceleration again.

Key words: *cavitation bubble*; *rigid wall*; *acoustic wave*; *compressible*

1. Introduction

In the free field, the cavitation bubble will expand violently and contract rapidly with the driving of acoustic wave. And the cavitation bubble will keep a near-spherical oscillation for multiple cycles under some frequencies and amplitudes. During the motion, with the high temperature and interior pressure, the cavitation bubble may emit the light as well as the noise, so called the sonoluminescence (Crum and Reynolds, 1985; Gaitan *et al*., 1992). The research on the motion characteristics of cavitation bubble induced by acoustic wave is concentrated on the experiment (Laborde *et al*., 1998; Lauterborn *et al*., 2007; Ohi *et al*., 1999) and spherical theory (Barber *et al*., 1997; Brenner *et al*., 1995).

Since the high-speed contraction after the driving of acoustic wave, the compressibility of fluid is important. Prosperetti and Lezzi (1986a, 1986b) modified the Rayleigh–Plesset equation (Rayleigh, 1917) for the consideration of compressibility with the integrated and refined derivation. However, the high-order Rayleigh–Plesset equation has an unphysical spurious unstable solution. The method to overcome this problem is put forward by Keller and Miksis (1980). Since in the form of Rayleigh–Plesset-type equation with sound radiation term, the Keller–Miksis equation has the higher precision (Prosperetti and Lezzi, 1986a), the theoretical analysis of sonoluminescence always uses it to solve the motion of spherical cavitation bubble.

However, the frequency or amplitude range of acoustic wave for the stable oscillation is just small

* The project was financially supported by the National Natural Science Foundation of China (Grant No. 51279038) and the Excellent Young Science Foundation of the National Natural Science Foundation of China (Grant No. 51222904).

1 Corresponding author. E-mail: zhangaman@hrbeu.edu.cn

(Lohse *et al.*, 1997), and the cavitation bubble becomes unstable and non-spherical out of the range (Calvisi *et al.*, 2007) or there is a rigid wall or free surface near it. Since the non-spherical motion cannot be solved analytically, the numerical method, for example, boundary element method (BEM) (Blake and Gibson, 1981; Wang, 2005), should be introduced. The BEM just needs to calculate the quantities on the boundary, and satisfies the boundary condition at infinity automatically without setting the artificial boundary condition, so it owns the high precision and efficiency. However, the classical BEM is based on the incompressible potential flow theory to solve the Laplace equation, as that the influence of compressibility is not taken into account. Calvisi *et al*. (2007) utilized the classical BEM to analyze the stability of cavitation bubble driven by the travelling acoustic wave with the consideration of heat exchange, diffusive equilibrium and chemical reaction. To make full use of the advantages of BEM, and to consider the compressibility of fluid, Wang and Blake (2010, 2011) added the modified terms for compressibility in the Bernoulli equation. With the classical BEM and modified Bernoulli equation, Wang solved the motion of non-spherical cavitation bubble driven by travelling acoustic wave (Wang and Blake, 2010) and standing acoustic wave (Wang and Blake, 2011) in the weak compressible fluid.

In this paper, by using wave equation, and combining the idea from DAA method (Doubly asymptotic approximations) (Geers, 1978, 1980), which matches the spherical wave solution and delay potential formula with low-order expansion in the frequency domain, the motion of cavitation bubble is divided into prophase and anaphase, and then matched with the help of Laplace transformation to consider the compressibility. Finally, the boundary integral equation is presented with the compressible modification. The dynamics of cavitation bubble in the free field driven by the travelling wave have been researched with this method (Yao *et al.*, 2013). In this paper, the case of the cavitation bubble near the rigid wall with the vertical incident acoustic wave is solved with the mirror theory and asymmetrical model. The influence of the driving frequency, driving amplitude, and the vertical distance between cavitation bubble and rigid wall on the dynamical characteristics is analyzed.

2. Basic Theory

2.1 Boundary Integral Equation in the Compressible Fluid

In the numerical model, we assume that the ideal fluid around is irrotational and compressible, and the motion procedure of cavitation bubble is adiabatic. Since the size of cavitation bubble is small enough within the level of micron, the gravitation and the buoyance are neglected. And also since the grid size is much smaller than the wave length of the acoustic wave, the one-way coupling model is utilized, i.e. the acoustic field is assumed not to be affected by the motion of cavitation bubble. The whole field satisfies the linear wave equation (Geers, 1978):

$$\nabla^2\varphi = \frac{1}{c^2}\varphi_{tt}\,, \tag{1}$$

where, φ is the velocity potential in fluid; for the small amplitude perturbation, $c \approx c_\infty$, c_∞ being the sound speed of the fluid without disturbance; the subscript means the corresponding partial derivative.

The schema of numerical method is shown in Fig. 1. When the motion time is small, the cavitation bubble shape approximates the sphere. The problem can be assumed to be in one-dimension along the

radial direction. Thus the prophase approximation for the motion can be expressed as (Zhang *et al*., 2013):

$$\varphi_t(r,\ t) = -c\kappa\varphi(r,\ t) - c\varphi_n(r,\ t)\,, \tag{2}$$

where, κ is the curvature of cavitation bubble surface; r is the radius. It is similar to the approximation done in the DAA method (Geers, 1978, 1980) at high frequency.

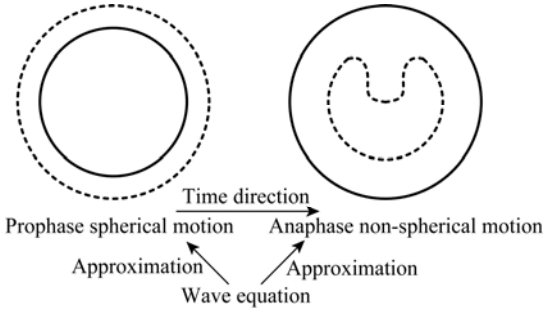

Fig. 1. Schema for the numerical method. The bubble shape is spherical at the prophase, but will be non-spherical at the anaphase; the motion in these two phases will be approximated by the wave equation, respectively. The solid line means the early time shape and the dash line means the later time shape.

Solve Eq. (1) with its Green function (Bluck and Walker, 1996), and when the motion time t is sufficiently large, such that $r_{pq}/(tc)$ is much smaller than 1, keep only the term of order $1/c$ for the solution after Taylor expansion. Thus, the anaphase approximation is obtained (Zhang *et al*., 2013):

$$\alpha\varphi\left(\boldsymbol{r}_p,t\right) = -\iint_{S(\tau)} \frac{r_{pq}\cdot\boldsymbol{n}_q}{r_{pq}^3}\varphi\left(\boldsymbol{r}_q,\tau\right)\mathrm{d}S - \iint_{S(\tau)} \frac{1}{r_{pq}}\varphi_n\left(\boldsymbol{r}_q,\tau\right)\mathrm{d}S + \frac{1}{c}\iint_{S(\tau)} \varphi_{nt}\left(\boldsymbol{r}_q,\tau\right)\mathrm{d}S\,. \tag{3}$$

where, $\boldsymbol{r}_p$ and $\boldsymbol{r}_q$ are the location vectors of field point and source point, respectively; r_{pq} is the distance between the field point and source point; t is the time for the field point, and τ is the source time; $\boldsymbol{v}$ is the velocity of cavitation bubble surface; α is the solid angle; $\boldsymbol{n}_q$ is the unit outward normal vector at the source point. It is similar with the approximation done with the DAA method (Geers, 1978, 1980) at low frequency. To solve the motion, the field point p and the source point q are all arranged on the surface. For convenience, Eq. (3) is rewritten as:

$$c\mathfrak{I}\varphi + c\mathfrak{O}\varphi_n = \mathfrak{R}\varphi_{nt}\,, \tag{4}$$

where, $\mathfrak{I}$, $\mathfrak{O}$, and $\mathfrak{R}$ are the corresponding coefficient matrixes. We match Eq. (2) and Eq. (4) with the help of Laplace transformation (Zhang *et al.*, 2013). Finally, the boundary integral equation in compressible fluid can be expressed as follows (Zhang *et al*., 2013):

$$\begin{aligned}\varphi_{tt} = &-c\left[\left(\mathfrak{O}^{-1}\mathfrak{I}-\kappa\right)\left(\boldsymbol{E}-\mathfrak{O}^{-1}\mathfrak{R}\mathfrak{O}^{-1}\mathfrak{I}\right)^{-1}+\kappa\right]\varphi_t - \left(\mathfrak{O}^{-1}\mathfrak{I}-\kappa\right)\left(\boldsymbol{E}-\mathfrak{O}^{-1}\mathfrak{R}\mathfrak{O}^{-1}\mathfrak{I}\right)^{-1}\mathfrak{O}^{-1}\mathfrak{I}c^2\varphi\\ &-c\left[\varphi_{nt}+c\left(\mathfrak{O}^{-1}\mathfrak{I}-\kappa\right)\left(\boldsymbol{E}-\mathfrak{O}^{-1}\mathfrak{R}\mathfrak{O}^{-1}\mathfrak{I}\right)^{-1}\varphi_n\right].\end{aligned} \tag{5}$$

The detail process of derivation for Eq. (5) can be found in Zhang *et al.* (2013). In Eq. (5), $\boldsymbol{E}$ is the identity matrix. Setting the sound speed in Eq. (5) to be infinite, we may obtain the boundary integral equation in incompressible fluid.

2.2 Acoustic Field Acting on the Cavitation Bubble

A cavitation bubble in equilibrium state is released near a rigid wall with the distance d, which is called the initial vertical distance hereafter. A reflected wave W_{R} is formed by a travelling incident plane

wave W_I, as shown in Fig. 2. The acoustic wave is along the z-axis, i.e. it is vertical to the rigid wall. And the point on the rigid wall that has the nearest distance to the initial cavitation bubble is defined as the center of the rigid wall. In this paper, the mirror method (Du *et al*., 2001) is adopted to simulate the cavitation bubble near the rigid wall. We set the incident wave $W_I=P_a\sin(-kz-\omega t+\theta_0)$ as the plane travelling wave along negative z-axis, and its total reflected wave $W_R=P_a\sin(kz-\omega t+\theta_0)$. After superimposing of the incident wave and its reflected wave, the standing wave field is generated at one side of the rigid wall (Du *et al*., 2001):

$$P_{st}=W_I+W_R=2P_a\cos(kz)\sin(\theta_0-\omega t), \tag{6}$$

where, P_a is the amplitude of the incident wave, which is called the driving amplitude hereafter; k is the wave number; $\omega=2\pi f$ is the circular frequency; f is the frequency of the incident wave, which is called the driving frequency hereafter; θ_0 is the initial phase.

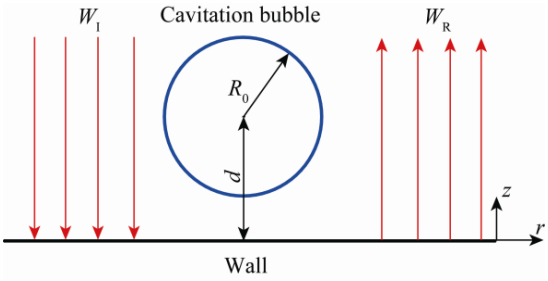

Fig. 2. Cavitation bubble and the sound field near the rigid wall, W_I is the incident wave and W_R is the reflected wave, and they make up the standing wave field.

The boundary condition for cavitation bubble can be expressed as the Bernoulli equation (Yao *et al*., 2013):

$$\frac{P_b}{\rho_\infty}+\varphi_t+\frac{1}{2}|\nabla\varphi|^2+u_a\nabla\varphi=0, \tag{7}$$

where, u_a is the velocity induced by the acoustic wave in the fluid; $P_b=P-P_{st}-P_\infty$, P_∞ is the pressure at infinity, and P is the pressure in fluid and also at the cavitation bubble surface:

$$P=P_v+P_0\left(\frac{V_0}{V}\right)^\gamma-M\kappa. \tag{8}$$

where, P_0 and V_0 are the initial inner pressure and volume of the cavitation bubble; P_v is the saturated vapor pressure; γ=1.4 is the gas specific heat in this paper; M=0.0728 N/m is the coefficient of surface tension. We notice that

$$\varphi_{Dt}=\varphi_t+(u_b+u_a)\nabla\varphi=\varphi_t+(\nabla\varphi)^2+u_a\nabla\varphi, \tag{9}$$

where, φ_{Dt} is the material derivative of velocity potential; u_b is the velocity induced by the cavitation bubble. The Lagrangian schema is adopted for Eq. (7) with Eq. (9):

$$\varphi_{Dt}+\frac{P_b}{\rho_\infty}=\frac{1}{2}|\nabla\varphi|^2. \tag{10}$$

By solving Eq. (5), Eq. (8) and Eq. (10) together, the motion of cavitation bubble near the rigid wall with the driving of acoustic wave is obtained. Since the vertically incident of travelling wave, the axisymmetric model is utilized in this paper, and the axis of symmetry is along z-axis. For precision,

the forth-order Runge–Kutta schema is utilized for the time marching. To avoid the nodes aggregation on the surface at the place with high curvature due to the large deformation, the technique called EMT (Elastic Mesh Technology) (Wang *et al*., 2003) is adopted to adjust the distance between the nodes. And to avoid the appearance of zigzag deformation because of the numerical instability at some places on the surface, the five-point smooth technique (Sun, 2007) is introduced at a few steps to keep the shape stability without obvious distortion.

3. Numerical Results and Discussion

3.1 Numerical Certification

3.1.1 *Acoustic Cavitation in the Unbounded Field*

To certificate the method presented in this paper, the motion of a single cavitation bubble under the driving of acoustic wave in unbounded compressible fluid is calculated, and compared with the result from Keller–Miksis equation (Keller and Miksis, 1980). To ensure the same acting pressure for the numerical simulation and the Keller–Miksis equation, we set z=0 and θ_0=0 in the incident wave W_I. And the driving term P_{st} in Eq. (7) is equal to the central acoustic pressure of the spherical cavitation bubble. The results shown in Fig. 3 certify that the method presented in this paper can solve the motion of cavitation bubble with the driving of acoustic wave precisely. And compared with the results of incompressible model, the oscillation radius of compressible model decreases obviously in time after the first oscillation.

We find that in Fig. 3a using compressible model, for one period, the motion of cavitation bubble has three stages. At first, it expands to the maximum radius due to the initial negative acting sound pressure. Then, it contracts because of the phase changing of acoustic wave and the large pressure in the fluid around. Finally, it oscillates near the initial radius (i.e. the equilibrium radius) with its natural frequency until the next period. Fig. 3b shows the inner pressure of cavitation bubble during the motion with the compressible model used in Fig. 3a.

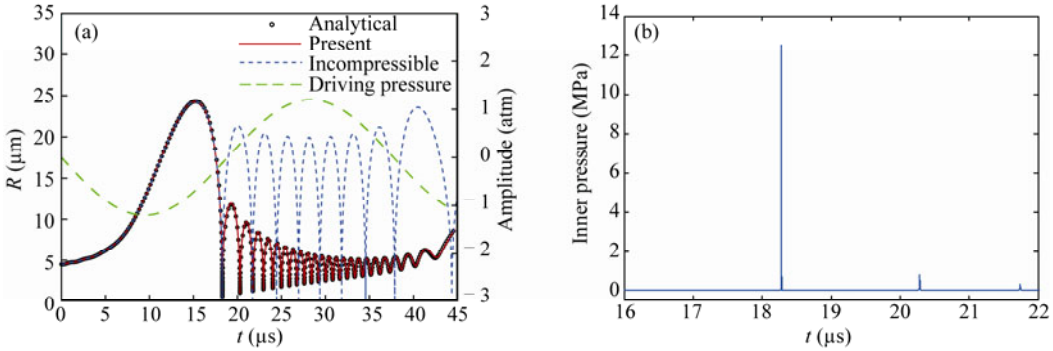

Fig. 3. Verification of the results from BEM with those of from the Keller–Miksis equation: (a) radius; (b) inner pressure using compressible model (f=26.5 kHz, ρ_∞=998 kg/m^3, c_∞=1500 m/s, P_∞=101.3 kPa, R_0=4.5 μm, P_v=2338 Pa, P_a=1.2P_∞, θ_0=0).

It indicates that when the cavitation bubble reaches its minimum volume, the inner pressure increases rapidly to a large value, and it is the same with the temperature (Brenner *et al*., 2002). Thus, the

extreme environment in the cavitation bubble is formed. If there is some percentage of inert gas inside the cavitation bubble, the bubble will emit the light stably during the multiple cycles oscillation, which is known as the single-bubble sonoluminescence (SBBL). But it should be noticed that SBBL just occurs under some strict conditions, such as suitable initial radius, inert gas content, medium around, driving frequency, and driving amplitude (Brenner *et al.*, 2002; Gaitan *et al.*, 1992).

3.1.2 *Comparison with the Experiment of Bubble near the Rigid Wall*

By using the method presented in this paper to solve the motion of bubble near the rigid wall with the driving amplitude P_a=0, the results are compared with the experimental data (Zhang *et al.*, 2011). The initial vertical distance is 10.4 mm and the maximum radius is 14.4 mm. The experimental results are shown in Fig. 4a, while the numerical results are shown in Fig. 4b. We find that the numerical method presented in this paper can well simulate the motion of bubble near the rigid wall.

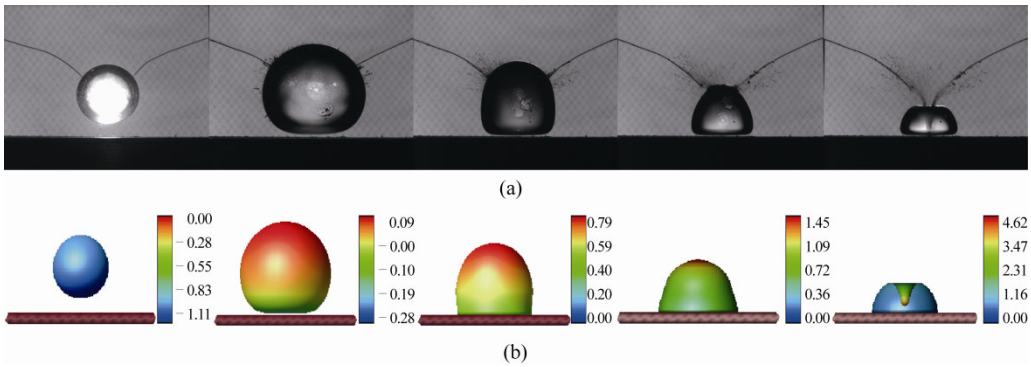

Fig. 4. Comparison between experiment (Zhang *et al.*, 2011) and numerical simulation: (a) experimental results (t=0.69, 2.41, 3.82, 4.25, 4.45 ms); (b) simulated results (t=0.62, 2.17, 3.46, 3.83, 4.01 ms, the contours represent the velocity potential on the surface of cavitation bubble, which is non-dimensional).

3.2 Cavitation Bubble near the Rigid Wall in Compressible Fluid with Driving of Acoustic Wave

A cavitation bubble in equilibrium state is released near the rigid wall, and its initial radius is R_0=15 μm, the driving amplitude is P_a=0.8 atm, and the driving frequency is set as 1.5 times the natural frequency of the same cavitation bubble in the free-field (Brennen, 1995) (224.5 kHz, called free natural frequency hereafter), the initial vertical distance is d=30 μm, and the initial phase is θ_0=π.

The numerical simulation and the characteristics analysis for the motion are stopped at the moment when the jet touches the other side of the cavitation bubble surface and begins to form the toroidal bubble (Zhang *et al.*, 2001).We call this moment the end of the jet stage in this paper. Furthermore, to analyze expediently, one oscillation is defined as a set of expansion and contraction stage.

Expanding the utilization of Indirect Boundary Element Method (IBEM) for the compressible fluid (Yao *et al.*, 2013), we can obtain the velocity potential at any near-field point without the second-order derivation. Then the pressure and velocity distribution in the near-field can be solved using the Bernoulli equation, as shown in Fig. 5. The corresponding history of equivalent radius (the radius for the sphere with same volume, and for convenience, it will just be called radius hereafter), inner pressure and the jet tip velocity are shown in Fig. 6. Fig. 5a shows the amplitude of the acoustic field near the rigid wall (t=0)

and the initial location of cavitation bubble; there is an antinode at the rigid wall, where the amplitude is the largest.

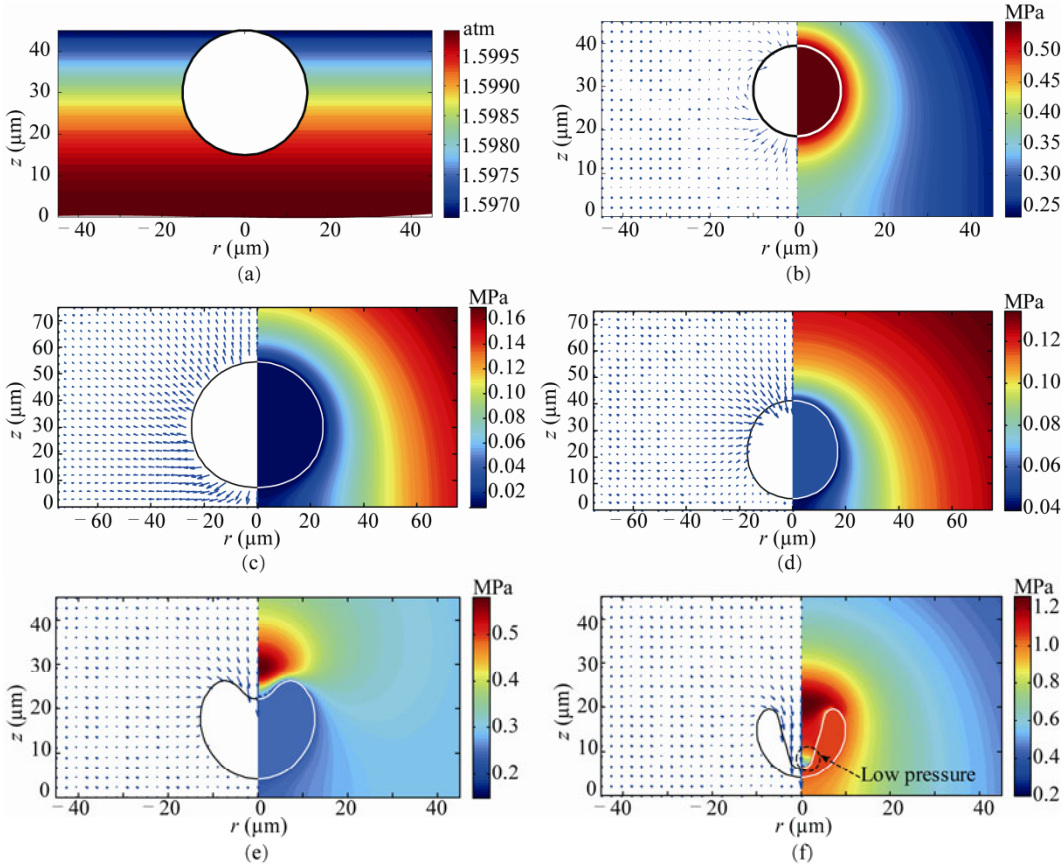

Fig. 5. Shape and distribution of velocity and pressure in fluid.

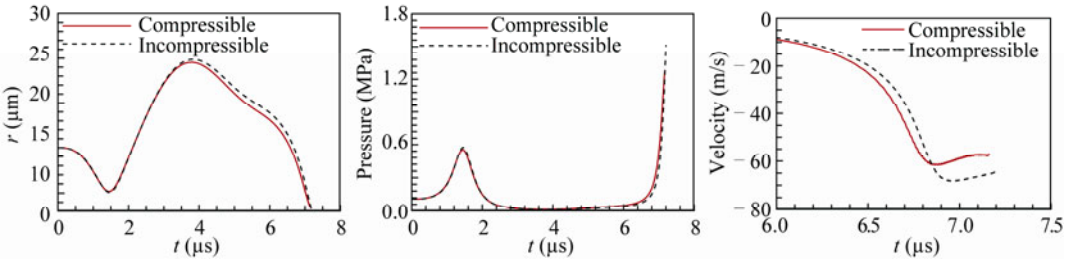

Fig. 6. Motion characteristics for compressible and incompressible model: (a) equivalent radius; (b) inner pressure; (c) jet tip velocity.

As known from Eq. (6), when the initial phase $\theta_0=\pi$, the driving pressure acting on the cavitation bubble surface is positive at the prophase, i.e. the direction of acoustic pressure points to the inner of bubble. So the bubble contracts at first. As shown in Fig. 5b, when the bubble first reaches the minimum volume, it still keeps spherical, and the inner pressure is larger than that in the fluid around. At this stage, the velocity near the wall has pointed to the fluid, while the velocity far from the wall still points to the

inner of bubble, i.e. the side of the bubble near the wall will expand earlier than other place. Subsequently, the bubble begins to expand. As shown in Fig. 5c, the bubble nearly reaches the maximum volume; the inner pressure is smaller than that in the fluid. And the velocity around the bubble and near the wall is larger than that at the side far from the wall, with the direction pointing to the fluid. After reaching the maximum volume, the bubble begins to contract again, as shown in Figs. 5d−5f. It can be seen from Fig. 5d that the side of bubble surface far from the wall converts into the contraction state firstly, and the velocity around here is much larger than that at other place. With the marching of the contraction, the jet is formed at the side far from the wall, and also pointing to the wall. As shown in Fig. 5e, at the prophase of the jet stage, the velocity in fluid near the jet is much larger than that at other places. There is a high pressure area near the jet, since the perturbation of velocity potential is severe here, and φ_t is negative with a large absolute value. Fig. 5f shows the bubble shape for the anaphase of jet stage, and at this moment, the jet is obvious and nearly touches the other side of the bubble. And near the jet tip, because of the large velocity, there is a low-pressure area.

As shown in Fig. 6, compared with the compressible model, the oscillation amplitude of incompressible model is larger. At the end of jet stage, the peak value of the inner pressure and jet tip velocity using incompressible model is larger than that using compressible model, since the energy in the near field will not propagate to the far field. Also, since the radius of the compressible model is not much different from the incompressible one, the influence of the rigid wall on this comparison is just small, i.e. the differences between the two models are mainly caused by the compressibility. According to Fig. 6c, the maximum jet tip velocity is 61.6 m/s, whose corresponding Mach number is 0.041, thus this case is weakly compressible.

3.3 Influence of Acoustic Wave Parameters on the Motion Characteristics of Cavitation Bubble

3.3.1 *Driving Amplitude*

Releasing a cavitation bubble near the wall, first we discuss the influence of the driving amplitude on the motion. The initial radius and initial vertical distance are set the same as in Section 3.2, the driving frequency is the free natural frequency (224.5 kHz), and the initial phase is θ_0=0. The history curves of radius with different driving amplitudes are shown in Fig. 7a, while the histories of radius with much smaller driving amplitudes are shown in Fig. 7b.

When the driving amplitude is small, the end of jet stage may be in the second expanding stage, such as P_a=0.5 atm. The average acoustic energy destiny of standing wave field is just related to the driving amplitude (Du *et al*., 2001), and is also small, which leads to the weak oscillation amplitude with larger minimum radius and smaller maximum radius. With the increment of the driving amplitude, the acoustic energy destiny increases, and the oscillation amplitude is amplified obviously, with the maximum radius enlarging and the minimum radius reducing. With the further increment of the driving amplitude, the radius is enlarged continuously. But the existence of the rigid wall will limit the further expansion of cavitation bubble, and will lead to the larger radius at the jet stage, so the minimum radius increases, and the oscillation amplitude is further weakened.

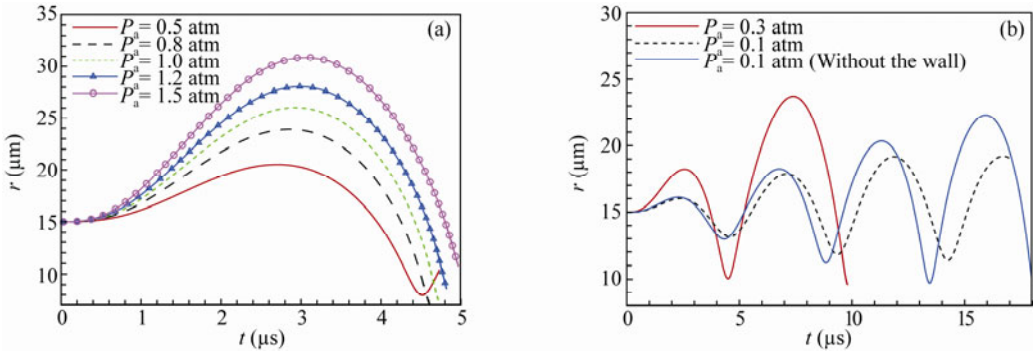

Fig. 7. History of radius with different driving amplitudes: (a) P_a=0.5, 0.8, 1.0, 1.2, 1.5 atm; (b) P_a=0.3, 0.1, 0.1 atm (without rigid wall).

For the case that the driving amplitude is quite small, as shown in Fig. 7b, the cavitation bubble keeps oscillation for multiple cycles before the forming of jet. In addition, to explain the influence of rigid wall on the motion of cavitation bubble further, we keep all the parameters unchanged (i.e. the standing acoustic wave is also not changed), and just remove the wall. The comparison is also shown in Fig. 7b. We can find more clearly that the existence of the rigid wall limits the increment of the maximum radius and the reduction of the minimum radius. Moreover, the time for one oscillation is also elongated with the rigid wall, i.e. the natural frequency of the cavitation bubble decreases near the wall.

Fig. 8 shows the history of jet tip velocity and the central pressure on the rigid wall with different driving amplitudes. Fig. 9 represents the comparison of the shape at the end of jet stage. With the increment of the driving amplitude, the jet tip velocity increases, with the 'robust' jet shape. Since the cavitation bubble is just near the wall, and the jet is formed at the side far from the wall, the variation of the central pressure on the wall is similar to the inner pressure. As shown in Eq. (8), it indicates that the inner pressure is related to the bubble volume directly. Thus, since the minimum volume decreases at first and then increases with the increment of the driving amplitude as shown in Fig. 7, the peak value of the central pressure on the wall increases at first and then decreases.

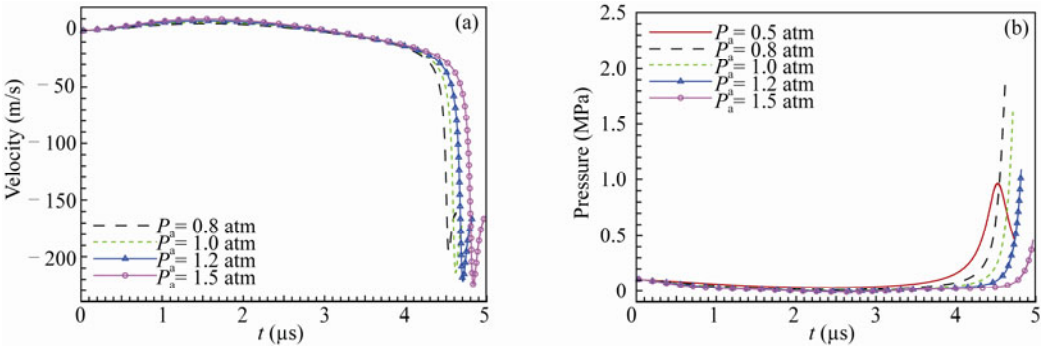

Fig. 8. History of motion characteristics with different driving amplitudes: (a) jet tip velocity, P_a=0.8, 1.0, 1.2, 1.5 atm; (b) pressure at the center of rigid wall, P_a=0.5, 0.8, 1.0, 1.2, 1.5 atm.

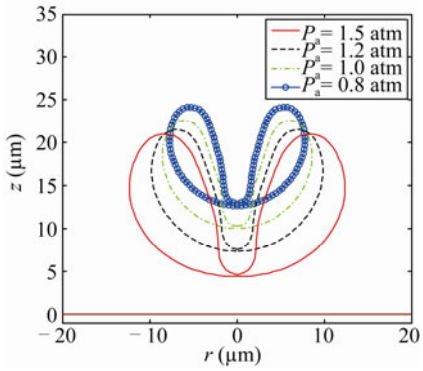

Fig. 9. Shape comparison at the end of jet stage for different driving amplitudes.

3.3.2 *Driving Frequency*

The influence of driving frequency on the motion of cavitation bubble is researched in this section. The initial radius and the vertical distance are the same as Section 3.3.1, with the driving amplitude P_a=1 atm, and the initial phase θ_0=0.

Fig. 10 shows the history of the radius with some driving frequencies. We define f^* as the ratio of the driving frequency to the free natural frequency. With the increment of driving frequency and the unchanged driving amplitude, due to the faster transition of the acoustic pressure phase, time for one oscillation is shortened, i.e. the motion state of cavitation bubble is transformed quickly. Thus, the radius fluctuates gently and gradually with the reduction of the maximum radius and the increment of the minimum radius.

However, because of the existence of the rigid wall, the increment of the maximum radius and the reduction of the radius at the jet stage are limited in reality. When the driving frequency is small, since the maximum radius is still large, the limitation of the rigid wall to the cavitation bubble is obvious, which leads to a larger radius at the jet stage even larger than the initial radius, i.e. the reduction of the radius at the jet stage is impeded. But the maximum radius decreases obviously with the increment of driving frequency, as shown in Fig.10, thus the oscillation amplitude is weakened. Subsequently, due to the continuous reduction of the maximum radius, the limitation of the wall to the motion is weakened gradually. Therefore, the radius at the jet stage decreases and is smaller than the initial radius, i.e. the minimum radius decreases. Finally, with the further increment of driving frequency, the large speed transformation of the motion state leads to the weakness of the oscillation amplitude but without large limitation from the wall due to the small radius during the motion.

Fig. 11 shows the history of the jet tip velocity, and Fig. 12 shows the history of the central pressure on the wall, while Fig. 13 represents the shape comparison at the end of the jet stage for different driving frequencies. It indicates that with the increment of the driving frequency, the jet tip velocity decreases, and the jet shape becomes ‘thin’. Combined with the analysis in Section 3.3.1 about the relation between the bubble volume and pressure on the center of the wall, the history of the central pressure on the wall shown in Fig. 12 can be illustrated. It shows that when the minimum radius is smaller than the initial radius, the peak value of the central pressure on the wall exits at the end of the jet stage, and with the increment of driving frequency, the peak value increases at first and then decreases according to the variation of the minimum radius.

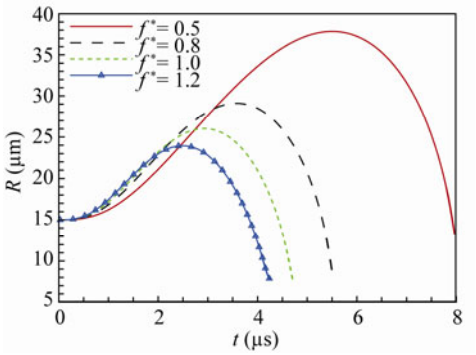

Fig. 10. Radius with different frequencies.

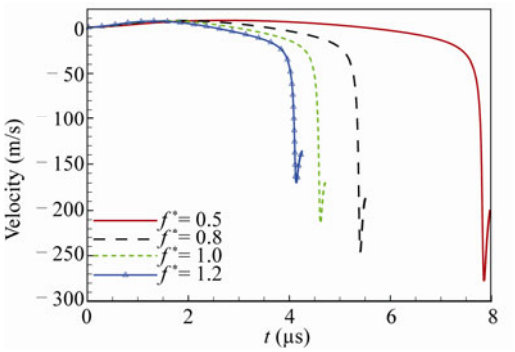

Fig. 11. Jet tip velocity with different frequencies.

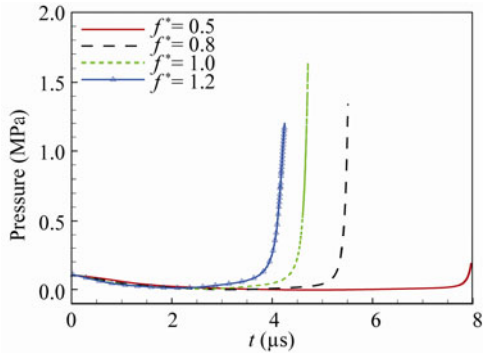

Fig. 12. Central pressure on the wall with different frequencies.

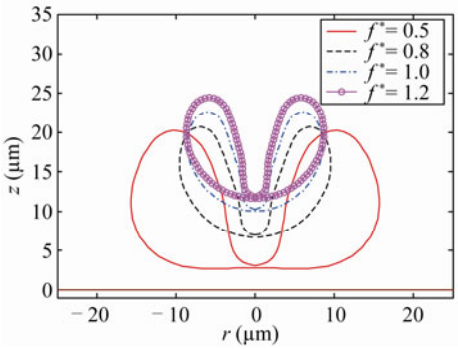

Fig. 13. Shape comparison at the end of the driving jet stage with driving frequencies.

3.4 Influence of Initial Vertical Distance on the Motion of Cavitation Bubble

The influence of initial vertical distance on the motion is researched in this section. We keep the initial radius and incident wave unchanged, and define the distance parameter for initial vertical distance as $\lambda=d/R_0$. In addition, we define $\lambda=\infty_r$ to represent the case that there is not a rigid wall near the cavitation bubble but just a driving acoustic wave in the free field; $\lambda=\infty_i$ represents the case that there is not a rigid wall, but the driving acoustic wave is the same as the case $\lambda=8$.

Fig. 14 represents the history of radius with λ=1.5, 2, 2.5, 3, 4, 8, ∞_r, and ∞_i, and the arrow in the figure means the increasing direction of λ. Fig. 15 gives the oscillation amplitude variation of the first oscillation with the increment of λ.

With the increment of λ, time for one oscillation decreases. It also indicates that the existence of rigid wall elongates the time for one oscillation as mentioned above. We notice that if the cavitation bubble is very close to the rigid wall, the expanding maximum radius will be limited, as well as the contraction minimum radius, which leads to a large radius at the jet stage, as shown in Fig. 14. With the increment of λ, since the limitation of rigid wall to the bubble volume decreases, the maximum radius increases, while the minimum radius decreases, thus the oscillation amplitude increases. When λ is large, the influence of the wall on the motion is weakened, i.e. the influence of λ on the motion is weak, which leads to small variation of the maximum and the minimum radius. Thus, the increment of the oscillation amplitude is slowed down. In addition, the end of the jet stage may be in the second expanding stage,

such as the curve shown in Fig. 14 when λ=8.

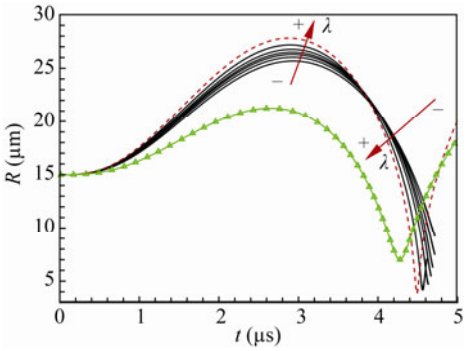

Fig. 14. Radius for different λ (λ=1.5, 2, 2.5, 3, 4, 8, ∞_i, and ∞_r; the red dash line represents $\lambda = \infty_i$, and "Δ" represents $\lambda = \infty_r$).

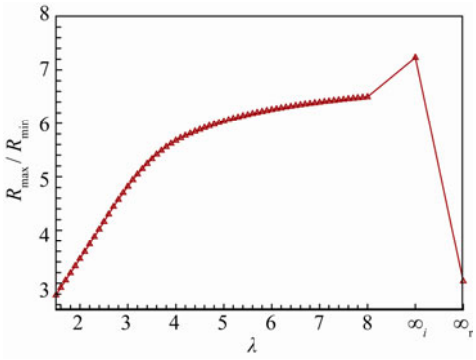

Fig. 15. Relation between oscillation amplitude and λ.

When $\lambda=\infty_r$, because of the absence of the rigid wall, which leads to the disappearance of the reflected wave, the driving amplitude acting on the cavitation bubble decreases obviously. Thus, the maximum radius decreases and the minimum radius increases, i.e. the oscillation amplitude is weakened. When $\lambda=\infty_i$, we may find that with the same acting acoustic wave but just removing the rigid wall, the limit to the cavitation bubble will be removed as well, which leads to larger maximum radius and smaller minimum radius compared with the case λ=8, i.e. the oscillation amplitude is amplified.

As discussed above, the existing rigid wall reflects the acoustic wave to generate the standing wave field and amplifies the acting acoustic wave. On the other hand, the rigid wall limits the expanding and contraction stage of the cavitation bubble.

Fig. 16 gives the shape history at the contraction stage when λ=1.5, 2, 2.5, and 3.5, respectively. When λ is small, the side of cavitation bubble near the wall is flat due to the repulsion of the rigid wall. With the increment of λ, as the limitation of the rigid wall is weakened, the flat shape disappears gradually.

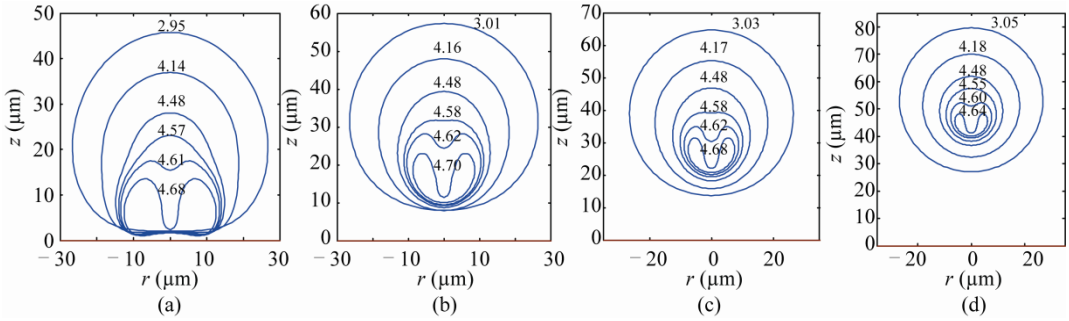

Fig. 16. Shape comparison of the cavitation bubble contraction with different λ (the numerals in the figures mean the motion time with unit of "μs"): (a) λ=1.5; (b) λ=2; (c) λ=2.5; (d) λ=3.5.

Fig. 17 represents the relation curves for the peak value of the jet tip velocity and λ. When λ is small, the attraction of the rigid wall to the jet is strong (Zhang *et al.*, 2011), which leads to a larger peak value of the jet tip velocity. Thus with the increment of λ, since the attraction to the jet is weakened, the

peak value of the jet tip velocity decreases. When λ is large, with the increment of λ, the development degree of the jet is improved, and thus the peak value is enlarged (Blake *et al.*, 1999). After the further increment of λ, the influence of the rigid wall on the cavitation bubble is weakened continuously. And the jet stage extends to the second expanding stage after the minimum radius has been reached, i.e. the jet speed is similar to, or even smaller than the expanding speed. So the peak value decreases. Thus altogether during the increment of initial vertical distance, the influence of rigid wall on the jet is first accelerating, then slowing down, and finally accelerating again.

To further investigate the impact of acoustic wave on the dynamics of the cavitation bubble near the rigid wall, we calculate the case without the driving of acoustic wave but with an initial inner pressure interior. With a larger initial inner pressure compared with the background pressure, the cavitation bubble can expand independently, and the equilibrium radius increases, which leads to a smaller free natural frequency (Brennen, 1995), i.e. a longer time for one oscillation. Here, we define the strength factor $\varepsilon=P_0/P_\infty$. The variation of the peak value of the jet tip velocity with λ is shown in Fig. 18. The strength factor ε=100 and the driving amplitude P_a=0 for this case, other parameters are the same as above. It indicates that with a small λ, the peak value decreases with the increase of λ, which is just contrary when λ is large. The similar conclusion can be found in Zhang *et al.* (2011) with the experiment. We can also find that the variation is similar to the case where the driving acoustic wave exists. Thus, whether there is a driving acoustic wave or not, the jet is accelerated by the rigid wall when the vertical distance is small and limited after the increment of the vertical distance.

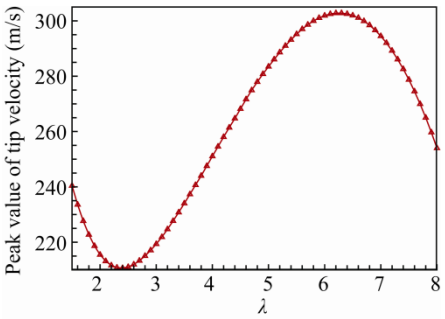

Fig. 17. Relation between the peak value of the jet tip velocity and λ.

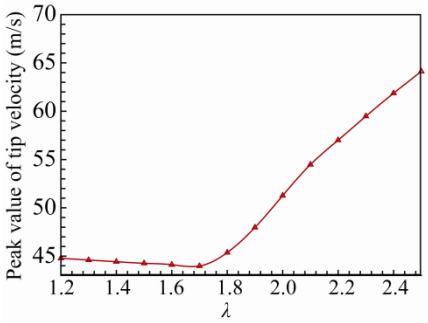

Fig. 18. Relation between the peak value of the jet tip velocity and λ.

The comparisons of the jet tip velocities between the cases with or without the acoustic wave driving are shown in Fig. 19 with ε=100, P_a=1 atm, and λ=4, 6. We notice that there are some small amplitude oscillations on the curves in Fig. 19, which are generated by the acoustic wave driving, because of the smaller acting sound pressure compared with the initial inner pressure, and the larger driving frequency compared with the free natural frequency of the cavitation bubble in these cases. When θ_0=0, the sound pressure acting on the cavitation bubble is negative at first, it may accelerate the expanding and lead to large limit from the rigid wall, which also impedes the contraction to reduce the peak value of the jet tip velocity smaller than that of the case without acoustic wave driving. When $\theta_0=\pi$, the acting sound pressure is positive at first, and it will weaken the expanding. Thus, small λ (λ=4, $\theta_0=\pi$) can cause small limit from the rigid wall, so the contraction is sufficient, i.e. the volume at the jet stage is

small, and the peak value of the jet tip velocity increases. However, for large λ (λ=6, θ_0=π), since the influence of the limit from the rigid wall on the cavitation bubble is small, the weak expanding does not cause obvious limit reduction but only leads to smaller jet tip velocity compared with other cases with the same λ.

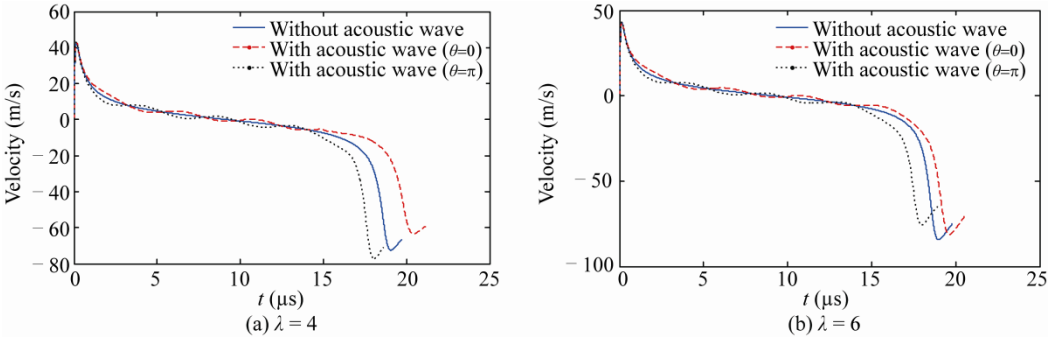

Fig. 19. Comparison of the jet tip velocity with or without acoustic wave.

4. Conclusions

Based on the wave equation, the prophase and anaphase of the cavitation bubble motion is matched with the help of Laplace transformation, and the modified boundary integral equation in compressible fluid is obtained. With the mirror method, the motion characteristics of the cavitation bubble near the rigid wall with the driving of standing wave field generated by the incident wave and its totally reflected wave are solved.

The cavitation bubble will expand or contract after the driving of acoustic wave, and finally form the jet pointing to the wall. With the numerical examples in this paper, we find that with the consideration of compressibility, time for the same counts of oscillation is shortened, and the oscillation amplitude is reduced, as well as the peak value of the inner pressure and jet tip velocity. With the increment of initial vertical distance, the limit from the rigid wall to the cavitation bubble is reduced, and the influence of the rigid wall on the jet is first accelerating due to the attraction; then slowing down due to the sufficient development being blocked; and finally accelerating again since the jet stage may be ended even after the minimum radius has been reached. Based on the discussion above, the influence of the driving frequency and amplitude on the motion of the cavitation bubble is discussed, which may be summarized as follows:

(1) Near the rigid wall, with the small driving amplitude or large driving frequency, the cavitation bubble may oscillate for multiple cycles.

(2) When the driving amplitude is large or the driving frequency is small, the limit from the wall is large, which impedes the expansion of the cavitation bubble, and leads to the large radius at the contraction stage.

(3) With the reduction of the driving frequency or the increment of the driving amplitude, the peak value of the jet tip velocity increases, and the peak value of the induced pressure on the center of the wall increases at first but then decreases because of the limit from the rigid wall to the motion of bubble.

References

Barber, B. P., Hiller, R. A., Löfstedt, R. A., Putterman, S. J. and Weninger, K. R., 1997. Defining the unknowns of sonoluminescense, *Phys. Reports*, **281**(2): 65–143.

Blake, J. R. and Gibson, D. C., 1981. Growth and collapse of a vapour cavity near a free surface, *J. Fluid Mech.*, **111**, 123–140.

Bluck, M. J. and Walker, S. P., 1996. Analysis of three-dimensional transient acoustic wave propagation using the boundary integral equation method, *Int. J. Numer. Meth. Eng.*, **39**(8): 1419–1434.

Brennen, J. R., 1995. *Cavitation and Bubble Dynamics*, Oxford University Press.

Brenner, M. P., Hilgenfeldt, S. and Lohse, D., 2002. Single-bubble sonoluminescence, *Reviews of Modern Physics*, **74**(2): 425.

Brenner, M. P., Lohse, D. and Dupont, T. F., 1995. Bubble shape oscillations and the onset of sonoluminescence, *Phys. Rev. Lett*., **75**, 954.

Calvisi, M. L., Lindau, O., Blake, J. R. and Szeri, A. J., 2007. Shape stability and violent collapse of microbubbles in acoustic traveling waves, *Phys. Fluids*, **19**(4): 047101–047115.

Crum, L. A. and Reynolds, G. T., 1985. Sonoluminescence produced by 'stable' cavitation, *J. Acoust. Soc. Am.*, **78**(1): 137–139.

Du, G. H., Zhu, Z. M. and Gong, X. F., 2001. *Acoustics Foundation*, Nanjing University Press, Nanjing, China. (in Chinese)

Johnson, E. and Colonius, T., 2008. Shock-induced collapse of a gas bubble in shockwave lithotripsy, *J. Acoust. Soc. Am.*, **124**(4): 2011–2020.

Gaitan, D. F., Crum, L. A., Church, C. C. and Roy, R. A., 1992. Sonoluminescence and bubble dynamics for a single, stable, cavitation bubble, *J. Acoust. Soc. Am.*, **91**(6): 3166–3183.

Geers, T. L., 1978. Doubly asymptotic approximation for transient motions of submerged structure, *J. Acoust. Soc. Am.*, **64**(5): 1500–1508.

Geers, T. L. and Felippa, C. A., 1980. Doubly asymptotic approximations for vibration analysis of submerged structure, *J. Acoust. Soc. Am*., **73**(4): 1152–1159.

Keller, J. B. and Miksis, M. J., 1980. Bubble oscillations of large amplitude, *J. Acoust. Soc. Am*., **68**(2): 628–633.

Laborde, J. L., Bouyer, C., Caltagirone, J. P. and Gérard, A., 1998. Acoustic bubble cavitation at low frequencies, *Ultrasonics*, **36**(1): 589–594.

Lauterborn, W., Kurz, T., Geisler, R., Schanz, D. and Lindau, O., 2007. Acoustic cavitation, bubble dynamics and sonoluminescence, *Ultrason. Sonochem.*, **14**(4): 484–491.

Lohse, D., Brenner, M. P., Dupont, T. F., Hilgefeldt, S. and Johnston, B., 1997. Sonoluminescing air bubble rectify argon, *Phys. Rev. Lett.*, **78**(7): 1359–1362.

Ohi, C. D., Kurz, T., Geisler, R., Lindau, O. and Lauterborn, W., 1999. Bubble dynamics, shock waves and sonoluminescence, *Phil. Trans. R. Soc. Lond*., *Ser. A*, **357**(1751): 269–294.

Prosperetti, A. and Lezzi, A., 1986a. Bubble dynamics in a compressible liquid. Part 1. First-order theory, *J. Fluid Mech.*, **168**, 457–478.

Prosperetti, A. and Lezzi, A., 1986b. Bubble dynamics in a compressible liquid. Part 2. Second-order theory, *J. Fluid Mech.*, **185**, 289–321.

Rayleigh, L., 1917. On the pressure developed in a liquid during the collapse of a spherical cavity, *The London, Edinburgh, and Dublin Philosophical Magazine and Journal of Science*, **34**(200): 94–98.

Sun, H., 2007. *A Boundary Element Method Applied to Strongly Nonlinear Wave-Body Interaction Problems*, Ph. D. Thesis, Norwegian University of Science and Technology, Trondheim.

Wang, C., Khoo, B. C. and Yeo, K. S., 2003. Elastic mesh technique for 3D BIM simulation with an application to underwater explosion bubbles, *Comput. Fluid.*, **32**(9): 1195–1212.

Wang, Q. X., 2005. Unstructured MEL modelling of nonlinear unsteady ship waves, *J. Comput. Phys.*, **210**(1): 368–385.

Wang, Q. X. and Blake, J. R., 2010. Non-spherical bubble dynamics in a compressible liquid. Part 1. Travelling acoustic wave, *J. Fluid Mech*., **659**, 191–224.

Wang, Q. X. and Blake, J. R., 2011. Non-spherical bubble dynamics in a compressible liquid. Part 2. Acoustic standing wave, *J. Fluid Mech*., **679**, 559–581.

Yao, X. L., Ye, X. and Zhang, A. M., 2013. Cavitation bubble in compressible free fluid subjected to the travelling wave, *Acta Phys. Sin.*, **62**(24): 244701-1–244701-11. (in Chinese)

Zhang, A. M., Wang, S. P., Bai, Z. H. and Huang, C., 2011. Experimental study on bubble pulse features under different circumstances, *Chinese J. Theor. Appl. Mech.*, **43**, 71–83. (in Chinese)

Zhang, A. M., Wang, S. P. and Wu, G. X., 2013. Simulation of bubble motion in a compressible liquid based on the three dimensional wave equation, *Eng. Anal. Bound. Elem*., **37**(9): 1179–1188.

Zhang, Y. L., Yeo, K. S., Khoo, B. C. and Wang, C., 2001. 3D jet impact and toroidal bubbles, *J. Comput. Phys*., **166**(2): 336–360.